Diffraction-anomalous-fine-structure spectroscopy applied to the study of III-V strained semiconductors

M. G. Proietti
Departamento de Física de la Materia Condensada and Instituto de Ciencia de Materiales de Aragón, CSIC, Universidad de Zaragoza, pza. S. Francisco s.n., 50009 Zaragoza, Spain

H. Renevier*
Laboratoire de Cristallographie, Centre National de la Recherche Scientifique, Boîte Postale 166, F-38042 Grenoble Cedex 09, France and Université Joseph Fourier, Boîte Postale 53, F-38041 Grenoble Cedex 09, France

J. L. Hodeau
Laboratoire de Cristallographie, Centre National de la Recherche Scientifique, Boîte Postale 166, F-38042 Grenoble Cedex 09, France

J. García
Instituto de Ciencia de Materiales de Aragón, CSIC, Universidad de Zaragoza, pza. S. Francisco s.n., 50009 Zaragoza, Spain

J. F. Bérar and P. Wolfers
Laboratoire de Cristallographie, Centre National de la Recherche Scientifique, Boîte Postale 166, F-38042 Grenoble Cedex 09, France
(Received 13 April 1998; revised manuscript received 29 July 1998)

The effect of built-in strain on III-V epitaxial semiconductors has been investigated by extended diffraction anomalous fine structure (EDAFS) at the Ga and As *K* edges. A general formalism is presented for analyzing the diffraction-anomalous-fine-structure (DAFS) oscillations, valid for any type of crystallographic structure. The EDAFS spatial selectivity provides a unique tool for studying systems that are out of the reach of other x-ray techniques. We study two different systems grown on a GaAs(001) substrate: a strained layer superlattice of $(GaP)_2(InP)_3$ and three single epilayers of $GaAs_{1-x}P_x$ ($x=0.20-0.23$) partially relaxed, with a different amount of residual strain. The bond distance Ga-P in the SLS is stretched by about 0.04 Å in agreement with the predictions of the elastic theory. The Ga-As and Ga-P bond lengths in $GaAs_{1-x}P_x$ remain very close to their respective bulk values, independent of the residual strain. The $GaAs_{1-x}P_x$ epilayers have also been measured by switching the light polarization vector from the [110] to the $[1\bar{1}0]$ crystallographic direction. An effect is observed on the EDAFS at the Ga *K* edge for the most strained sample, suggesting an ordering of the P atoms in the [001] growth direction. We also point out the interest of the DAFS spectra analysis for obtaining further information about the average crystallographic structure. [S0163-1829(99)06307-9]

I. INTRODUCTION

Strained semiconductors have been widely studied due to their extensive application in the technology of electronic and optoelectronic devices.[1] High-quality, dislocation-free materials can be obtained, allowing the fabrication of high-performance devices of increasing complexity. In this sense the contribution of mismatched heteroepitaxy is twofold since it allows either a wider range of compositions and the presence of strain itself can induce changes in the electronic properties of the materials,[2] providing a further degree of freedom in the device design. Nevertheless, the greatest effort in characterizing this class of material has been devoted to the study of their optical and electronic properties, whereas their local atomic structure has not been extensively studied.

If the thickness of the epilayer is lower than some ''critical'' thickness, the strain can be accommodated through a tetragonal deformation of the crystalline lattice. When the critical layer thickness is exceeded, the generation of misfit dislocations becomes energetically favorable, releasing the strain generated at the interface and inducing a lattice relaxation. In that case a severe degradation of the material quality occurs in terms of device performance. Since the critical thickness and the strained cell parameters can be estimated according to different models,[3–5] a direct measurement of the local structural parameters of the strained materials can provide a check of the limits of application of the theory.

Extended absorption fine structure (EXAFS) would be the most suitable technique for getting information about the short-range structure of these compounds, and it has indeed been successfully applied both to pseudobinary bulk alloys and strained samples.[6–10] Here EXAFS cannot be applied in a straightforward way, i.e., in transmission or fluorescence mode, because the epitaxial samples are often much too thin to be measured in transmission or are grown on a substrate having some of the atomic components in common with the epilayer. Alternative approaches as glancing-angle EXAFS or surface EXAFS (SEXAFS) have been used[11–13] but they solve the problem only in part, since the signal collection is restricted to very thin surface layers.

The aim of this work is to study the structural properties of different strained III-V semiconductors samples using the alternative approach provided by the DAFS spectros-

copy.[14–21] DAFS combines the local structural sensitivity of x-ray absorption fine structure (XAFS) with the long-range crystallographic sensitivity of x-ray diffraction (XRD) by measuring Bragg peak intensities as a function of energy through an absorption edge. The energy-dependent modulation of the diffraction intensity contains local structural information that is chemical and valence specific similar to that of XAFS. The advantage of DAFS for studying epilayers or multilayers is to give selective structural information by choosing the Bragg peaks (spatial-selective Bragg peak) of the strained phase and the heterostructure is probed through the entire thickness. Interfaces in superlattices have also been studied by using the site selectivity of DAFS.[16]

The samples we measured represent two different regimes of strain. In one case, the sample is a strained layer superlattice (SLS) of $(GaP)_2(InP)_3$ grown on a GaAs(001) substrate. The subindexes 2 and 3 refer to the number of atomic monolayers (ML) constituting the individual GaP and InP layers. Each component has a large mismatch with GaAs (-3.6% for GaP, $+3.8\%$ for InP) giving rise to a large biaxial deformation in the individual layers. The strain alternates from tensile for GaP to compressive for InP, so its net value in the SLS is very small, favoring structural stability. The strain is supposedly accommodated by deformation of the lattice since the individual layer thickness is lower than the critical thickness.

In the second case, the samples are single epilayers of $GaAs_{1-x}P_x$, grown also on a GaAs(001) substrate, with a P concentration of about 20%, and different thicknesses, ranging from 600 to 5000 Å. X-ray-diffraction measurements show the presence of a ''residual'' in-plane strain, defined as $\varepsilon_{\parallel}=(a_{\parallel}-a_0)/a_0$, $a_{\parallel}$ being the in-plane lattice parameter, and a_0 the lattice parameter of the bulk alloy. The amount of residual strain decreases with increasing epilayer thickness, and it is related to the strain-induced Raman shift of the GaAs-like and GaP-like vibrations, as reported for the same samples.[22] The strain-induced Raman shift of the GaAs vibrational mode is greater than that observed for the Ga-P mode. A possible reason could be that the variation of the Ga-As bond length is larger than the Ga-P one as a function of the residual strain. EDAFS measurements can provide a direct measurement of the Ga-As and Ga-P interatomic distances to be compared with the Raman results and with the predictions of the elastic theory.

In the first part of this paper, we present a general formalism for analyzing the EDAFS oscillations which is valid for any type of crystallographic structure. In most cases, treatment of EDAFS and EXAFS data may be very similar. In the second part of the paper the DAFS spectra are analyzed with the program DPU (Data Processing Utility), written by one of us (P.W.), to obtain information about the average crystallographic structure and the above-mentioned method is applied to analyze the EDAFS oscillations. An EXAFS-like single shell analysis is performed using experimental model phases and amplitudes, to study the nearest neighbor (NN) environment. A multishell analysis, using theoretical phases and amplitudes generated by the GNXAS program,[23] including multiple scattering (MS) paths, is used to study the next-nearest neighbor (NNN) shell.

We also compare spectra of $GaAs_{1-x}P_x/GaAs$ epilayers recorded with [110] and $[1\bar{1}0]$ x-ray light polarization directions. These directions are not equivalent for the zinc-blende structure and the shape of the EDAFS spectrum changes appreciably for the most strained and thinnest epilayer.

II. FUNDAMENTALS OF DAFS ANALYSIS

A. DAFS analysis

In that section we present the different methods to recover local structural information via the analysis of the DAFS spectra obtained experimentally from the energy-dependent variation in the diffraction intensity near an absorption edge. Depending on the crystallographic site selectivity of the Bragg reflections, two different kinds of situations are encountered when analyzing the DAFS spectra. The easiest situation is the single-anomalous-site analysis which corresponds to only one anomalous crystallographic site contributing to the diffracted intensity. The XAFS-like structural information may be obtained without knowing the crystallographic structure and for instance an iterative Kramers-Kronig method may be used. The other and more tedious situation is the multiple-anomalous-sites analysis, which corresponds to several anomalous sites contributing to the diffracted intensity, with different weights. In that case a precise knowledge of the crystallographic structure is needed to extract the XAFS-like information about each anomalous sites.

In the forward scattering limit, the atomic scattering factor of an atom A on site j may be split above the edge into a smooth part and an oscillatory part:[14,18]

$$f_{Aj}(\mathbf{Q},E)=f_{0A}(\mathbf{Q})+f'_{0A}(E)+if''_{0A}(E)+\Delta f''_{0A}(E)[\chi'_{Aj}(E)+i\chi''_{Aj}(E)], \tag{1}$$

where f_{0A} is the Thomson scattering, f'_{0A} and f''_{0A} are the ''bare'' atom anomalous corrections to f_{0A}, and $\Delta f''_{0A}$ is the contribution of the bare resonant electronic transition alone, $\mathbf{Q}$ is the scattering vector, E is the energy of the incident beam, and $\chi'_{Aj}(E)+i\chi''_{Aj}(E)$ is the complex fine structure, which is the correction to the scattering factor due to the local atomic environment of the anomalous atom; χ''_{Aj} is formally identical to the EXAFS χ oscillations (optical theorem). For a general noncentrosymmetric structure where N_A is the number of anomalous atoms, the structure factor may be written

$$F(\mathbf{Q},E)=F_T(\mathbf{Q},E)e^{i\varphi_T(\mathbf{Q})}+\sum_{j=1}^{N_A}|\alpha_{Aj}(\mathbf{Q})|e^{i\varphi_{Aj}(\mathbf{Q})}[f'_{Aj}(E)+if''_{Aj}(E)], \tag{2}$$

where $f'_{Aj}=f'_{0A}+\Delta f''_{0A}\chi'_{Aj}$, $f''_{Aj}=f''_{0A}+\Delta f''_{0A}\chi''_{Aj}$, $F_T(\mathbf{Q},E)$ is a complex structure factor of phase φ_T that includes the net contribution of all nonanomalous atoms and the Thomson scattering of all anomalous atoms (see Fig. 1), $\alpha_{Aj}(\mathbf{Q})=c_{Aj}e^{-M_{Aj}Q^2}e^{i\varphi_{Aj}(\mathbf{Q})}$, $\varphi_{Aj}=\mathbf{Q}\cdot\mathbf{r}_j$, $|\alpha_{Aj}(\mathbf{Q})|=(\alpha_{Aj}\alpha^*_{Aj})^{1/2}$, c_{Aj} is the occupation factor of atom A on site j, and $\exp(-M_{Aj}Q^2)$ the crystallographic Debye-Waller factor, hereafter called the DW factor.

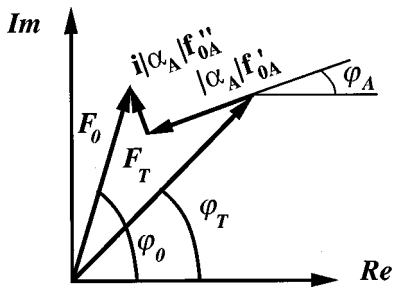

FIG. 1. Schematic drawing of the ''smooth'' structure factor F_0 decomposition used in the present paper. The subscript T refers to the contribution of all non anomalous atoms plus the Thomson scattering contribution of all anomalous atoms.

The measured intensity is proportional to the modulus squared of the structure factor ($|F|^2$) times several correction terms:

$$I(\mathbf{Q},E)=S\cdot D(E)\cdot A(\mathbf{Q},E)\cdot L(\mathbf{Q},E)\cdot P(\mathbf{Q})\cdot|F(\mathbf{Q},E)|^2, \tag{3}$$

where S is a scale factor; D takes into account the detector efficiency; A is the correction for the bulk absorbance of the sample together with the geometrical effects; L and P are the Lorentz and polarization corrections. We will call hereafter $F_0(\mathbf{Q},E)$ the complex smooth structure factor and $\varphi_0(\mathbf{Q},E)$ its phase, calculated without taking into account the complex fine structure and assuming that the bare atom anomalous corrections (f'_{0A},f''_{0A}) are identical for all anomalous atoms (Fig. 1). Then it can be easily shown from Eq. (2) that

$$|F_0(\mathbf{Q},E)|^2=|F_T|^2\{[\cos(\varphi_T-\varphi_A)+\beta f'_{0A}]^2 + [\sin(\varphi_T-\varphi_A)+\beta f''_{0A}]^2\}, \tag{4}$$

where $\beta=|\alpha_A|/|F_T|$ and $|\alpha_A|e^{i\varphi_A}=\Sigma_{j=1}^{N_A}\alpha_{Aj}e^{i\varphi_{Aj}}$.

Expression (4) shows that the energy-dependent variations of the diffracted intensity near an absorption edge give access to the phase difference $\Delta\Phi=\varphi_T-\varphi_A$ and the ratio β. Therefore they give important and precise information on the crystallographic structure. The shape of the DAFS spectrum is entirely determined by these two values. For instance the diffracted intensity goes down before the edge as long as $\cos(\Delta\Phi)$ is positive and is larger than the negative function $\beta f'_{0A}$ (see Fig. 1).

When a single anomalous site contributes to a reflection, the square of the modulus of the structure factor $F(\mathbf{Q},E)$ may be expressed by substituting in Eq. (4) $f'_A=f'_{0A}+\Delta f''_{0A}\chi'_A$ and $f''_A=f''_{0A}+\Delta f''_{0A}\chi''_A$ for f'_{0A} and f''_{0A}, respectively. An iterative Kramers-Kronig procedure may be used to extract χ'_A and χ''_A, starting with f'_{0A} and f''_{0A} (convoluted with a Lorentzian function to approximate the experimental resolution and the core-hole lifetime). Then the χ''_A oscillations are analyzed with a standard EXAFS data analysis package. The EXAFS-like structural information is obtained without the need of the crystallographic structure, and the second-order terms χ'^2_A and χ''^2_A are not neglected. That procedure consists of solving Eq. (4) at each energy for χ'_A (or χ''_A), then using the Kramers-Kronig transform to obtain χ''_A (or χ'_A) and repeating the iteration until convergence is reached. It should be pointed out that the iteration must be applied on χ'_A and χ''_A and not on f'_A and f''_A, except if $\varphi_0-\varphi_A\approx\varphi_T-\varphi_A$.

For a noncentrosymmetric structure with several anomalous sites, an expression as simple as Eq. (4) cannot be found because of the crossing terms $f'_{Aj}f''_{Ak}$ $(j\neq k)$: the iterative Kramers-Kronig procedure cannot be applied.

B. First-order EDAFS analysis

Alternatively a general formalism to analyze the EDAFS oscillations in a way very similar to an EXAFS analysis may be used. From Eqs. (1) and (2), the structure factor $F(\mathbf{Q},E)$ is divided into smooth and oscillatory parts:

$$F(\mathbf{Q},E)=F_0e^{i\varphi_0}+\Delta f''_{0A}(E)\sum_j|\alpha_{Aj}|e^{i\varphi_{Aj}}[\chi'_{Aj}+i\chi''_{Aj}]. \tag{5}$$

Then

$$\begin{aligned}|F(\mathbf{Q},E)|^2=&|F_0|^2+2|F_0||\alpha_A|\Delta f''_{0A}\\ &\times\sum_{j=1}^{N_A}w_{Aj}[\cos(\varphi_0-\varphi_{Aj})\chi'_{Aj}\\ &+\sin(\varphi_0-\varphi_{Aj})\chi''_{Aj}]\\ &+\Delta f''^2_{0A}|\alpha_A|^2\sum_{j=1}^{N_A}w^2_{Aj}(\chi'^2_{Aj}+\chi''^2_{Aj})\\ &+\Delta f''^2_{0A}|\alpha_A|^2\sum_{j=1,k>j}^{N_A}2w_{Aj}w_{Ak}\cos(\varphi_{Aj}-\varphi_{Ak})\\ &\times(\chi'_{Aj}\chi'_{Ak}+\chi''_{Aj}\chi''_{Ak})\\ &+\Delta f''^2_{0A}|\alpha_A|^2\sum_{j=1,k>j}^{N_A}2w_{Aj}w_{Ak}\sin(\varphi_{Aj}-\varphi_{Ak})\\ &\times(\chi'_{Aj}\chi''_{Ak}-\chi''_{Aj}\chi'_{Ak})\end{aligned} \tag{6}$$

where $w_{Aj}=|\alpha_{Aj}|/|\alpha_A|$.

The second-order terms may often be neglected for a variety of reasons: (a) the first-order EDAFS oscillations are multiplied by the modulus of the structure factor F_0, whereas the second-order terms are not, (b) the amplitude of $\chi'_{Aj}(\chi''_{Aj})$ decreases as $1/k$ whereas the second-order terms as $(1/k)^2$, (c) also the amplitude of $\chi'_{Aj}(\chi''_{Aj})$, usually of approximately 0.1, is ten times larger than the second-order terms. Neglecting the second-order terms, the first-order EDAFS oscillations $\chi_{\mathbf{Q}}(k)$ for a given scattering vector $\mathbf{Q}$ can be extracted directly out of the experimental spectrum and normalized according to the following formula:

$$\begin{aligned}\chi_{\mathbf{Q}}(k)=&\sum_{j=1}^{N_A}w_{Aj}[\cos(\varphi_0-\varphi_{Aj})\chi'_{Aj}+\sin(\varphi_0-\varphi_{Aj})\chi''_{Aj}]\\ =&\frac{|F_0|}{2|\alpha_A|\Delta f''_{0A}}\left(\frac{I_{\text{expt}}-I_{0\ \text{expt}}}{I_{0\ \text{expt}}}\right)\end{aligned} \tag{7}$$

where $k=\hbar^{-1}[2m(E-E_0)]^{1/2}$ is the photoelectron wave number, I_{expt} is the experimental intensity corrected for the

fluorescence background and the absorption of the incident and diffracted x-ray beams, $I_{0\ \mathrm{expt}}$ is the smooth background of the experimental EDAFS oscillations. Note that the contrast of the EDAFS oscillations, i.e., the relative amplitude of the fine structure to the Bragg peak intensity, is proportional to the ratio $|\alpha_A|/|F_0|$.

The DAFS normalization factor $S_D=|F_0|/(2|\alpha_A|\Delta f''_{0A})$, the phase difference $\varphi_0-\varphi_{Aj}$, and the weights w_{Aj} are calculated from the crystallographic structure. Another way to obtain the normalization factor is by fitting the DAFS spectrum with Eq. (4), so that

$$S_D=\{[\cos(\Delta\Phi)+\beta f'_{0A}]^2 + [\sin(\Delta\Phi)+\beta f''_{0A}]^2\}^{1/2}/[2\beta\Delta f''_{0A}]. \quad (8)$$

One procedure for extracting the site-selective structural information via χ'_{Aj} and χ''_{Aj} is to solve a linear system of the form of Eq. (7) at each energy by using the Kramers-Kronig transforms as an additional constraint to relate χ'_{Aj} and χ''_{Aj}.[16] This procedure is basically the same as refining the individual f'_{Aj} and f''_{Aj} at each energy,[20] except that the second-order terms are neglected. Generally the number of DAFS spectra is not much larger than the number of unknowns variables. Therefore, it is necessary to process reflections for which the contributions to the diffracted intensities of each anomalous site (w_{Aj}) are rather different, otherwise the linear system is not well conditioned. In addition, the coefficients w_{Aj} and the phases $\varphi_0-\varphi_{Aj}$ must be well known. Note that for a centrosymmetric structure the contribution of an atom A_j is exactly equal to zero when $\varphi_{Aj}=\pi/2$. This never happens for a noncentrosymmetric structure.

Refining the individual $f'_{Aj}(\chi'_{Aj})$ and/or f''_{Aj} (χ''_{Aj}) is the same as considering each value of χ'_{Aj} (χ''_{Aj}) to be independent as a function of the energy. That is obviously not true: in the EDAFS region the complex fine structure due to an atom A on site j may be written as an expansion over the scattering paths of the photoelectron around the absorbing atom:[14]

$$\chi'_{Aj}+i\chi''_{Aj}=-\sum_{\Gamma}\mathrm{Amp}^{\Gamma}_{Aj}(k)\exp\{-i[2kR^{\Gamma}_{Aj}+\delta^{\Gamma}_{Aj}(k)]\} \quad (9)$$

where χ''_{Aj} is equivalent to the EXAFS signal and χ'_{Aj} is related to χ''_{Aj} via the Kramers-Kronig transform, k is the the photoelectron wave number, Γ a photoelectron scattering path, $\mathrm{Amp}^{\Gamma}_{Aj}(k)$ is the net amplitude of the photoelectron scattering process, $\delta^{\Gamma}_{Aj}(k)$ is the net photoelectron scattering phase shift and R^{Γ}_{Aj} the effective path length. The real part χ'_{Aj} of the complex fine structure is a sum of cosine functions, and the imaginary part χ''_{Aj} is a sum of sine functions. From Eqs. (7) and (9), the EDAFS oscillations $\chi_{\mathbf{Q}}(k)$ can therefore be written with an expression very similar to the EXAFS one:

$$\chi_{\mathbf{Q}}(k)=\sum_j\sum_{\Gamma} w_{Aj}(\mathbf{Q})\mathrm{Amp}^{\Gamma}_{Aj}\sin[2kR^{\Gamma}_{Aj}+\delta^{\Gamma}_{Aj}(k) + \varphi_0(\mathbf{Q},k)-\varphi_{Aj}(\mathbf{Q})-\pi/2]. \quad (10)$$

Equation (10) shows that the EDAFS data can be treated as EXAFS data, provided that the crystallographic weights w_{Aj} and the phases $\varphi_0-\varphi_{Aj}$ to be added to the photoelectron phase shift can be calculated. The advantages of this analysis are (a) to introduce a parametrization of the DAFS oscillations and thereby to reduce the number of unknowns, (b) to allow a clean extraction of the EDAFS oscillations out of the experimental DAFS spectra, as required for the subsequent analysis of the nearest-neighbor shells, (c) to avoid the use of the Kramers-Kronig iterative method.

With a single anomalous site, the phase difference $\varphi_0-\varphi_A$ in Eq. (10) can be obtained directly from the fit of the smooth part of the DAFS spectrum:

$$\cos(\varphi_0-\varphi_A)=[\cos(\Delta\Phi)+\beta f'_{0A}]/\{[\cos(\Delta\Phi)+\beta f'_{0A}]^2 + [\sin(\Delta\Phi)+\beta f''_{0A}]^2\}^{1/2} \quad (11)$$

and

$$\sin(\varphi_0-\varphi_A)=[\sin(\Delta\Phi)+\beta f''_{0A}]/\{[\cos(\Delta\Phi)+\beta f'_{0A}]^2 + [\sin(\Delta\Phi)+\beta f''_{0A}]^2\}^{1/2}. \quad (12)$$

Once again the crystallographic structure is not necessary. In this situation the direct method using Eq. (7) is an easy way to analyze the DAFS spectrum and recover the XAFS-like information about the anomalous atom.

C. Centrosymmetric structure

For a centrosymmetric structure with several anomalous sites, the structure factor may also be written in a form similar to Eq. (4):[19]

$$|F(\mathbf{Q},E)|^2=|F_T|^2\{[\cos(\varphi_T)+\beta f'_A]^2+[\sin(\varphi_T)+\beta f''_A]^2\}, \quad (13)$$

where

$$f'_A=f'_{0A}+\Delta f''_{0A}\sum_{j=1}^{N_A} m_{Aj}w_{Aj}\cos(\varphi_{Aj})\chi'_{Aj}=f'_{0A}+\Delta f''_{0A}\chi'_A,$$

$$f''_A=f''_{0A}+\Delta f''_{0A}\sum_{j=1}^{N_A} m_{Aj}w_{Aj}\cos(\varphi_{Aj})\chi''_{Aj}=f''_{0A}+\Delta f''_{0A}\chi''_A,$$

$$\beta=\alpha_A/|F_T|,\quad w_{Aj}=|\alpha_{Aj}|/\alpha_A$$

and

$$\alpha_A=\sum_{j=1}^{N_A} m_{Aj}|\alpha_{Aj}|\cos(\varphi_{Aj}).$$

The summation runs over all atoms in the cell that are not related through the center of symmetry. Here, m_{Aj} is a multiplicity factor equal to 1 if the corresponding atom is at the origin of the cell, else $m_{Aj}=2$. An iterative Kramers-Kronig procedure may be used to extract χ'_A and χ''_A.[19] With several anomalous sites the structure must be known to determine the weights $w_{Aj}\cos(\varphi_{Aj})$ of the different sites and to recover the site-dependent χ'_{Aj} and χ''_{Aj}.

The first-order DAFS oscillations $\chi_{\mathbf{Q}}(k)$ in Eq. (7) may be written

TABLE I. Best-fit values of the parameters $\Delta\Phi$ and β obtained for the reflections 006 of the three $GaAs_{1-x}P_x$ layers at the Ga and As K edges. The direct method means that $\Delta\Phi$ and β were directly recovered by fitting Eq. (4) to the DAFS spectra. These parameters are compared to those calculated with the crystallographic structure.

	Ga K edge			As K edge
Sample	3	1	2	1
Thickness t (Å)	5000	4000	600	4000
Strain ε	0.4%	0.6%	0.7%	0.6%
$\Delta\Phi$	−29.9(2)	−8.7(7)	31.6(2)	−87.1(7)
β	0.68(4)	0.55(2)	0.58(2)	0.198(1)
(direct method)				
$\Delta\Phi$	$-27.4\rightarrow-19$	$-5\rightarrow-2.7$	$32\rightarrow24.1$	$-79.3\rightarrow-86$
β	$0.75\rightarrow0.59$	$0.58\rightarrow0.45$	$0.6\rightarrow0.45$	$0.2\rightarrow0.22$
(structure-based)				

$$\chi_{\mathbf{Q}}(k)=\sum_{j=1}^{N_A} m_{Aj}w_{Aj}\cos(\varphi_{Aj})[\cos(\varphi_0)\chi'_{Aj}+\sin(\varphi_0)\chi''_{Aj}]. \tag{14}$$

Equation (10) then becomes

$$\chi_{\mathbf{Q}}(k)=\sum_j \sum_\Gamma m_{Aj}w_{Aj}\cos(\varphi_{Aj})\mathrm{Amp}^\Gamma_{Aj} \times\sin[2kR^\Gamma_{Aj}+\delta^\Gamma_{Aj}(k)+\varphi_0(\mathbf{Q},k)-\pi/2]. \tag{15}$$

III. EXPERIMENT

The samples have been grown on semi-insulating GaAs(001)-oriented substrates by atomic layer molecular beam epitaxy (ALMBE). The growth details are reported elsewhere.[24] The XRD spectra of the 004 and 115 Bragg reflections, taken to measure the lattice parameters perpendicular and parallel to the surface, show that the epilayer Bragg peaks are well visible and well separated from the substrate peaks.

For the $GaAs_{1-x}P_x$ epilayers, the thicknesses range from 600 to 5000 Å and the amount of residual strain from 0.7 to 0.4%, as listed in Table I. The nominal P content was 23% for samples 1 and 2 and 20% for 3. The overall thickness of the $(GaP)_2(InP)_3$ SLS was 2500 Å.

The DAFS experiments were carried out at the French CRG (Collaborative Research Group) beamline D2AM (Diffraction Diffusion Multi-longueurs d'onde) at the ESRF (European Synchrotron Radiation Facility). The D2AM beamline[25] has been dedicated to anomalous scattering experiments and is well suited for performing DAFS experiments. Silicon (111) single crystals were used for the beam monochromatisation. We performed the experiments at the Ga and As K edges, 10.367 and 11.867 keV, respectively, with an energy resolution better than 1 eV. We used 500-Å-thick silicon photodiodes in photovoltaic mode for monitoring the incident beam and measuring the diffracted intensity. The fluorescence signal was recorded with a NaI scintillator or a photodiode. The spectra were recorded in a top-DAFS scan mode, i.e., always measuring the maximum intensity of the Bragg reflection as a function of energy. They were collected with the x-ray polarization vector normal to the scattering plane (σ-scattering geometry). The stability of both the beamline and the diffractometer with respect to width of the Bragg peaks (the full widths at half-maximum were approximately 0.05°) as well the mosaicity of the sample were sufficient to achieve a satisfactory signal-to-noise ratio with a reasonable integration time: a DAFS scan of one Bragg peak was about 2 h long.

IV. DAFS ANALYSIS

A. $GaAs_{1-x}P_x$ epilayers

The noncentrosymmetric $GaAs_{1-x}P_x$ structure is face-centered cubic with one atom (Ga) at the origin and the others (As and P) at $\frac{1}{4}, \frac{1}{4}, \frac{1}{4}$. From the structure factor for the 006 reflection $\{F\propto f_{\mathrm{Ga}}-xf_{\mathrm{As}}-(1-x)f_{\mathrm{P}}+i[f''_{\mathrm{Ga}}-xf''_{\mathrm{As}}-(1-x)f''_{\mathrm{P}}]\}$, one expects a large anomalous effect because the Thomson scattering contributions of Ga and As almost cancel out. The DAFS spectra at the Ga K edge measured with the 006 reflection of two $GaAs_{1-x}P_x$ samples (2 and 3) are shown in Fig. 2. The raw DAFS data at the Ga and As K edges, obtained from the 006 Bragg reflection of sample 1, are reported in Fig. 3. The signal-to-noise ratio is better than 0.5%. Note that the diffracted intensity, both at the Ga and As K edges, may be more than one order of magnitude larger than that measured 200 eV below the edge. Due to this very

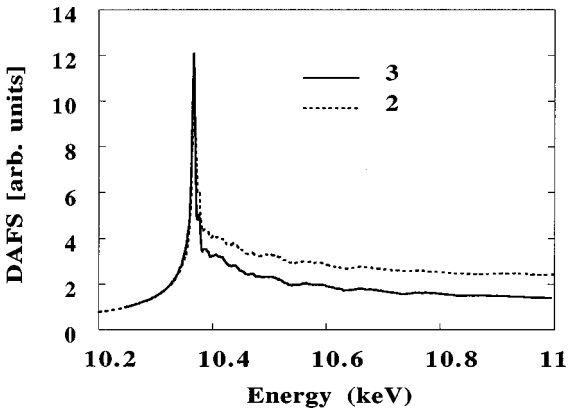

FIG. 2. DAFS spectra of the $GaAs_{1-x}P_x$ layers 3 and 2 taken with reflection 006 at the Ga K edge. The spectra were normalized to have the same relative intensity as the two spectra obtained with Eq. (4) and the values of $\Delta\Phi$ and β determined for each sample.

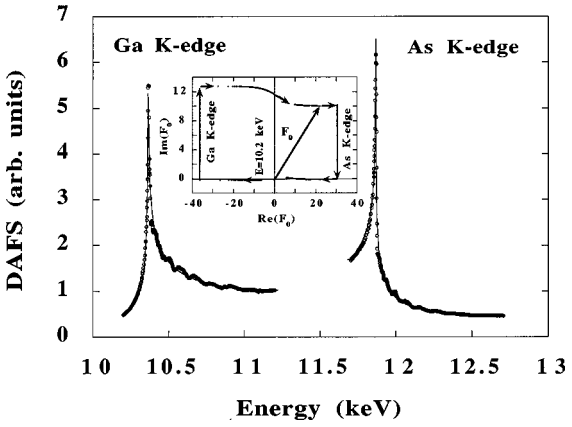

FIG. 3. DAFS spectra of a $GaAs_{1-x}P_x$ layer (sample 1) taken with reflection 006 at the Ga and As *K* edges. Open circles, raw data; solid line, best fit of the structure-based corefinement at the two edges. In inset is the $\mathrm{Im}(F_0)$ vs $\mathrm{Re}(F_0)$ showing the modulus and phase dependence of the structure factor (without the DAFS oscillations).

large anomalous effect, it turns out that the absorption correction is very small for all the samples, even for the thickest one. For instance, the relative absorption correction jump at the Ga K edge varies from 1.235 for the 5000-Å-thick sample to 1.03 for the 600-Å-thick. These are very small corrections compared to the relative anomalous variation at the edge of 15 (i.e., for the 006 reflection the effective absorption length is $2t/\sin(\theta) \approx 1.7\ \mu\mathrm{m}$). As already stated, for a single anomalous site system, the knowledge of the parameters $\Delta\Phi = \varphi_T - \varphi_A$ and β is sufficient for calculating the EDAFS normalization factor and the phase correction. They can be obtained by fitting Eq. (4) to the DAFS spectra. We also performed a crystallographic refinement of the spectra. The advantages of the structure-based refinement are (a) to take into account the exact crystallographic structure for calculating the absorption correction, (b) to allow the corefinement of the DAFS spectra at different edges, (c) to evaluate the EDAFS second-order terms contribution to the structure factor with respect to the first-order terms one. We find that for the 006 reflection the second-order term is at most 1% of the first-order term. It is worth noting that the 006 reflection is a weak one and it is not *a priori* a favorable case for neglecting the second-order term. Thus the approximation is valid.

At a given edge, the assumption that $\Delta\Phi$ and β are constant is not strictly true because the anomalous contribution to F_T changes smoothly as a function of the energy. Typically, at the Ga *K* edge, $\Delta\Phi$ and β vary at most by 8° and 25%, respectively, over an energy range of 600 eV after the edge. These variations at the Ga *K* edge result from the fact that Ga and As atoms are close to each other in the periodic table, their *K* edges being only 1.5 keV apart. There are basically two reasons for the overall shapes of the 006 DAFS spectra at the Ga and As *K* edges, (a) the crystallographic phases of the Ga and As sites are, respectively, 0 and 180°, (b) the difference between their atomic numbers *Z* is only 2, leading to a large β value. With the help of Fig. 1 and Eq. (4), one can easily understand the shapes. At the Ga *K* edge, $\Delta\Phi \approx -15°$, $\varphi_{A=\mathrm{Ga}} = 0$ and $\varphi_T \approx -15°$. $|F_T|$ is small compared to $|\alpha_{\mathrm{Ga}}| f'_{\mathrm{Ga}}$ giving a β value of about 0.5–0.7. Therefore the large contribution of $|\alpha_{\mathrm{Ga}}| f'_{\mathrm{Ga}}$ lead to a negative and decreasing real part of the structure factor, hence the diffracted intensity increase before the edge. After the edge, $|\alpha_{\mathrm{Ga}}| f'_{\mathrm{Ga}}$ starts to increase again, and the diffracted intensity decreases. At the As *K* edge $\Delta\Phi \approx -80°$, $\varphi_{A=\mathrm{As}} = 180°$, and $\varphi_T \approx 100°$. The large contribution of $|\alpha_{\mathrm{As}}| f'_{\mathrm{As}}$ leads to a positive and increasing real part of the structure factor so that the diffracted intensity increases before the edge. After the edge $|\alpha_{\mathrm{As}}| f'_{\mathrm{As}}$ starts to increase again, and the diffracted intensity decreases. In the inset of Fig. 3, the variations of the modulus and phase of the structure factor F_0 are represented as a function of the energy at the Ga and As *K* edges.

The refined values of the parameters $\Delta\Phi$ and β at the Ga and As *K* edges of the 006 DAFS spectra for the three strained epilayers are reported in Table I. The results obtained by the direct method using Eq. (4) and by the crystallographic refinement method are compared. In both cases, the diffracted intensity was multiplied by the structure-based absorption correction calculated with the bare atom anomalous terms $f''_{0\mathrm{Ga}}$ and $f''_{0\mathrm{As}}$. The sample thickness could not be refined due to the low effect of absorption on the spectra. The detector efficiency was assumed to be linear versus the energy and this was taken into account by multiplying the calculated intensity by a straight line that could tilt around a point of coordinates $(E_{\mathrm{edge}},1)$, its slope was refined. It should be noted that, to avoid a correlation between the slope and the parameters $\Delta\Phi$, the spectrum should extend far beyond the edge where the anomalous effect gets small. Also, the overall detector efficiency can be measured with a reflection that is not sensitive to the anomalous atoms.

What pertinent information about the crystallographic structure can we recover from the 006 DAFS spectra of the $GaAs_{1-x}P_x$ samples measured at both Ga and As *K* edges? According to Eq. (4) the two spectra give four parameters, i.e., $(\varphi_T)_{\mathrm{Ga}} - \varphi_{\mathrm{Ga}}$, β_{Ga}, $(\varphi_T)_{\mathrm{As}} - \varphi_{\mathrm{As}}$, β_{As}. Knowledge of these parameters is not enough to determine the crystallographic structure; however, they give a strong constraint on the real structure. The refinement based on the known structure of $GaAs_{1-x}P_x$ clearly showed that the spectra were very sensitive to the crystallographic Debye-Waller factor (DW) of the anomalous atoms, but the P concentration was correlated to the P, As, and Ga DW factors. It was impossible to refine these parameters together without any other assumptions. The best fit (with all correlation below 0.70) was obtained by constraining the DW's of the Ga and As to be equal. The refinement showed high correlation if only one edge was used and the best solution did not fit at the other edge. The best structure-based corefinement of the 006 DAFS spectra at the Ga and As *K* edges of sample 1 is shown in Fig. 3. The root mean square displacements of both Ga and As atoms were found to be equal to 0.4 Å, and the P concentration equal to 0.33.

The 006 DAFS spectra at the Ga *K* edge of the thinnest and thickest $GaAs_{1-x}P_x$ layers (2 and 3) are reported in Fig. 2. The spectra were normalized to the same relative intensity as the two spectra obtained with Eq. (4). The values of $\Delta\Phi$ and β are reported in Table I. The figure shows that the DAFS intensity of the thinnest sample (2) levels off after the edge at a higher value than the intensity of the other one (3). The difference is appreciable and cannot be explained by the

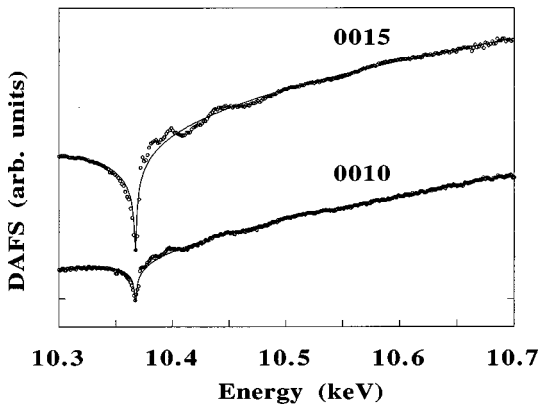

FIG. 4. SLS sample: DAFS spectra of reflections 0010 and 0015 (open circles) and the best fits of the structure-based corefinement (solid line).

lower absorption. It corresponds to a large increase of the phase difference $\Delta\Phi$ of about 60° and a decrease of β of about 0.1 (see Table I). Indeed, it is a signature of two slightly different crystallographic structures. From the refinement, it was clear that a slight displacement of the Ga atoms off the nominal z positions by $\Delta z = 0.0017$, i.e., less than 0.01 Å, is sufficient to explain the large increase of the phase difference $\Delta\Phi$ (z is the reduced atomic coordinate along the c axis of the cell, i.e., the growth direction, z is about 0 or 0.5). Such a difference could also be explained by a displacement of the As atoms towards the Ga of the same order of magnitude. The reason why the 006 is so sensitive results from the fact that the contribution of all atoms to F_T almost cancel each other. Therefore a tiny change in the crystallographic structure (or in the scattering power at the edge) gives rise to a large modification of the structure factor, either in modulus and/or phase. In the present case, a small displacement of the Ga atoms towards the As leads to a large Φ_T variation ($\Phi_A \approx 0$ and $|F_T|$ is almost constant). The small variation observed is comparable with the variation predicted by the elastic theory, as shown in Sec. V. This result shows the very high sensitivity of the 006 DAFS spectra to tiny details of the structure.

B. InP/GaP SLS

Regarding the SLS, the corefinement of the 0010 and 0015 DAFS spectra was based on a simple structural model. The noncentrosymmetric cell along the growth direction was built up by 10 atomic planes stacked according to the sequence: P-Ga-P-Ga-P-In-P-In-P-In. For the 0010 reflection, successive atomic planes contribute in phase whereas for the 0015, the phase difference is equal to 180°. There are actually two Ga sites which contribute with an equal weight ($w_{Aj} = 0.5$) to both the 0010 and 0015 reflections. Considering the simple structural model described above, which is in agreement with the DAFS measurements, the two Ga sites must have an identical near-neighbor environment. Therefore, we have made the assumption that the fine structure was identical for both sites.

The best fit of the two reflections (Fig. 4) is achieved with this simple structural model by increasing the root-mean-square displacement of the In atoms up to 0.09 Å. Refining other parameters such as the Ga Debye-Waller factor, a small atomic displacement, or an atomic mixing, did not lead to a better fit. Table II shows the values of $\Delta\Phi$ and β obtained with the direct method using Eq. (4) and the structure-based method. These two parameters are very stable as a function of the energy. The result shows once again the high sensitivity of the DAFS spectra to the crystallographic Debye-Waller factors.

TABLE II. Best-fit values of the parameters $\Delta\Phi$ and β obtained for the SLS $(GaP)_2(InP)_3$ sample at the Ga for the 0010 and 0015 reflections. The direct method means that $\Delta\Phi$ and β were recovered by fitting Eq. (4) to the DAFS spectra. These parameters are compared to those calculated with the crystallographic structure.

SLS $(GaP)_2(InP)_3$	Ga K edge	
Reflection	0010	0015
$\Delta\Phi$	2.5(7)	6.5(4)
β	0.0135(4)	0.0299(4)
(direct method)		
$\Delta\Phi$	3.8→3.5	7.1→6.4
β	0.012→0.012	0.0305→0.0306
(structure-based)		

V. EDAFS ANALYSIS: RESULTS AND DISCUSSION

A. Data reduction

The EDAFS spectra at the Ga and As K edges of one of the $GaAs_{1-x}P_x$ epilayers (sample 1) and of the SLS are shown in Fig. 5 together with GaAs and GaP transmission EXAFS spectra. The EDAFS amplitudes have been normalized according to expression (7) after a standard spline background removal. The SLS EDAFS spectrum in Fig. 5 is quite similar, as expected, to the bulk model, although less structured. The $GaAs_{1-x}P_x$ alloy spectrum is similar in shape and frequency to the GaAs model but it reveals the presence of P as backscatterer in the low-k region.

As stated above, the parameters $\Delta\Phi$ and β refined from the 006 DAFS spectra at the Ga K edge were not constant. Therefore, the EDAFS normalization factors (S_D) and the crystallographic phase shifts ($\varphi_0 - \varphi_A$) entering into the EDAFS expression [Eq. (7)], were calculated using the crystallographic structure. Figure 6 shows the EDAFS phase shifts $\varphi_0 - \varphi_{Ga} - \pi/2$ with respect to an EXAFS signal, at the Ga and As K edges for the 006 reflection of sample 1, as a function of the wave vector k of the photoelectron. At the Ga K edge the phase shift ranges from 50° to 0° in the whole k range, showing that the oscillations on the DAFS spectrum are sensitive to both χ'_{Ga} and χ''_{Ga} at low k value but very sensitive to χ''_{Ga} at k around 10 $Å^{-1}$. At the As K edge the phase shift is about 90° in the whole k range, the oscillations on the DAFS spectrum looks like $-\chi'_{As}$.

The comparison among the $GaAs_{1-x}P_x$ samples with different amount of residual strain is shown in Fig. 7 at the Ga K edge. The spectra are quite similar to each other, showing slight differences in the low-k region of the spectrum, more sensitive to the presence of P. All the spectra shown in Figs. 5 and 7 have been recorded with the x-ray beam polarization vector directed along the [110] crystallographic direction.

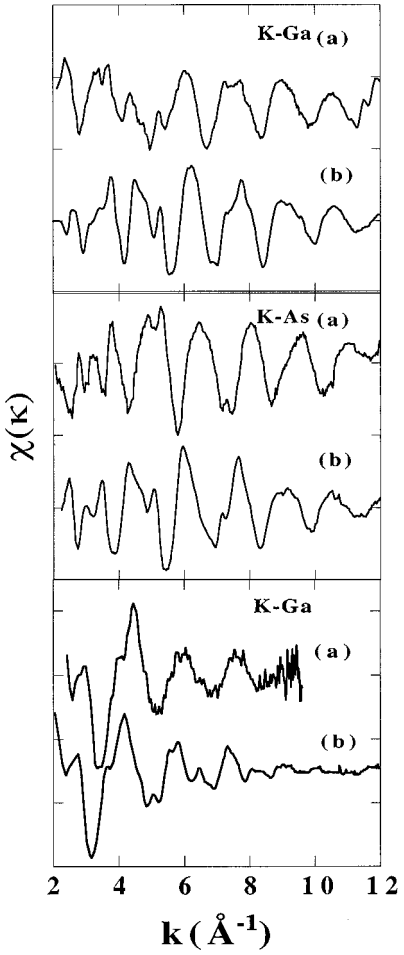

FIG. 5. Upper panel: EDAFS spectra at the Ga *K* edge of sample 1 (a) compared with the EXAFS, recorded in transmission mode, of bulk GaAs; (b) second panel, as above but at the As *K* edge; lower panel, SLS EDAFS spectrum at the Ga *K* edge (a) compared with transmission EXAFS of bulk GaP (b).

We performed DAFS measurements on two of the $GaAs_{1-x}P_x$ samples (1 and 2) also rotating the samples of 90° around the normal to surface ([001] direction) to align the polarization vector along the $[1\bar{1}0]$ direction, that is not equivalent to [110] for the noncentrosymmetric zinc-blende

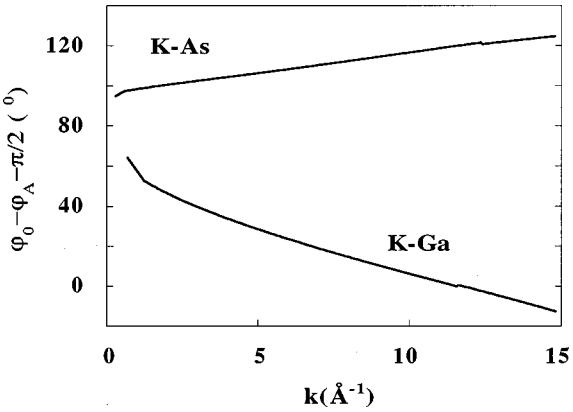

FIG. 6. $GaAs_{1-x}P_x$/GaAs sample: Phase shifts (with regards to an EXAFS signal) of the 006 EDAFS oscillations at the Ga and As *K* edges.

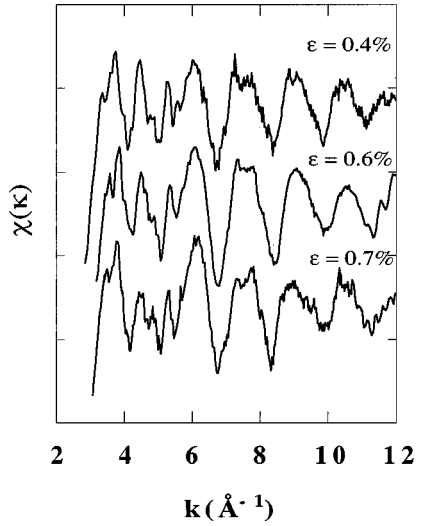

FIG. 7. Ga *K*-edge spectra of samples 3, 1, and 2, from upper to lower curve, respectively, recorded with the x-ray polarization vector directed along the same crystallographic direction ([110]).

structure. The EDAFS spectra recorded in the two polarization orientations are compared in Fig. 8 for samples 1 (upper panel) and 2 (lower panel). In the first case only very slight changes are observed, in agreement with a random distribution of the P atoms in the lattice, while for sample 2 which is the most strained and thinnest one, we can easily note an appreciable difference in the low-*k* region of the spectrum. Looking at the overall shape of the spectra, the EDAFS measured with the beam polarization along the $[1\bar{1}0]$ direction is much similar to GaAs, as if the P were less visible in the local Ga environment.

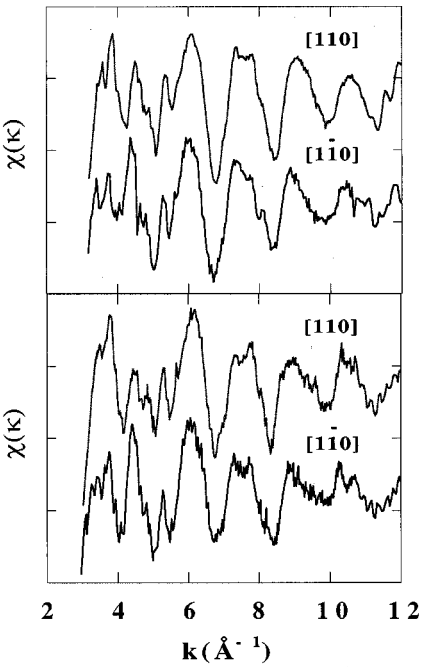

FIG. 8. Ga *K*-edge spectra of samples 1 (upper panel) and 2 (lower panel), recorded with the X-ray polarization vector directed along the [110] crystallographic direction and along the $[1\bar{1}0]$ crystallographic direction.

TABLE III. First shell best-fit values obtained for coordination numbers (N), interatomic distances (R) and the mean-square disorder in the bond-length factors (difference with the model) $\Delta(\Delta\sigma^2)$, for the two samples studied. The errors on N and $\Delta\sigma^2$ are $\Delta N/N = 30\%$, $\Delta(\Delta\sigma^2) = 0.002$ Å^2.

Sample	Abs. edge	Pair	N	R (Å)	$\Delta(\Delta)\sigma^2$ (Å^2)
SLS	Ga K	Ga-P	4.0	2.40 ± 0.01	-0.003
1	Ga K	Ga-As	2.2	2.43 ± 0.01	-0.003
1	Ga K	Ga-P	0.8	2.37 ± 0.02	0.001
1	As K	As-Ga	3.6	2.44 ± 0.01	0.002

B. SLS samples

A best-fit procedure, using experimental phases and amplitudes of bulk GaP, was performed on the filtered first shell contribution of the SLS EDAFS spectrum. The model phases were corrected according to expressions (10). The fit results are reported in Table III and shown in Fig. 9(a) at the Ga K edge. The errors on the fit parameters have been evaluated calculating the standard deviation corresponding to a normalized χ^2 value of about 2 (i.e., $N_{\rm ind}/\nu$, where $N_{\rm ind}$ is the number of independent points and ν is the difference between $N_{\rm ind}$ and the number of fit parameters). The χ^2 was calculated introducing on the filtered experimental curve an experimental error of approximately 4% i.e., of the same magnitude as the relative experimental error, which is in this case equal to 3.6%. That error was calculated by averaging the absolute value of the difference between the experimental χ values and the smooth signal obtained by Fourier filtering the data in the range 0–5 Å. The average estimated $\sigma_{\rm exp}$ was then divided by the average absolute value of χ.

The Ga-P bond length for the SLS sample, obtained from the first shell analysis, is $r_{\text{Ga-P}} = 2.40 \pm 0.01$ Å. We measure a difference $\Delta r = 0.04$ Å with respect to the bulk value of 2.36 Å. The built-in strain due to the lattice mismatch between GaP and GaAs is 3.6%, and the sample is still pseudomorphic. We can estimate, according to the elastic theory, the perpendicular lattice parameter

$$a_\perp = a^{\text{Ga-P}} + 2(C_{12}/C_{11})(a^{\text{Ga-P}} - a^{\text{Ga-As}}) = 5.271 \ \text{Å}$$

with $a^{\text{GaP}} = 5.541$ Å and $a_\parallel = a^{\text{Ga-As}} = 5.654$ Å,

In this case we have only one kind of atomic pair and we can calculate the strained Ga-P bond length from $r_s = 1/4(2a_\parallel^2 + a_\perp^2)^{1/2} = 2.394$ Å, which we can compare with the bulk alloy value for the $In_{1-x}Ga_xP$ ($x = 0.4$) $r_0 = 2.383$ Å. The EDAFS Ga-P bond length is in fair agreement with the strained bond length of 2.39 Å predicted by the elastic theory, showing that even for such a thin layer (2 ML) the theory still holds, as observed for other binary highly strained systems.[13] The $\Delta\sigma^2$ value is close, as expected, to that of the bulk compounds (Table III). No NNN shells analysis was performed on the SLS spectrum since the contribution of coordination shells beyond the first one was negligible. This is due not only to a signal-to-noise ratio that is not very high, but also to the presence of In as NNN atoms (in the InP adjacent layers), which interfere destructively with the NNN Ga atoms contribution.

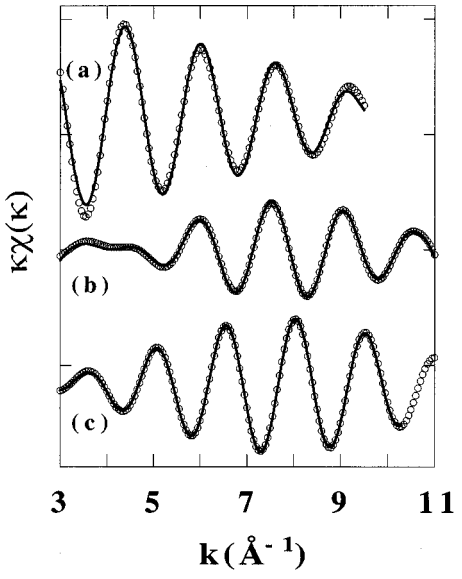

FIG. 9. Best-fit curve (solid line), obtained using experimental model phases and amplitudes, and filtered first shell contribution (circles) at the Ga K edge for the SLS sample (a) and sample 1 (b), and at the As K edge for sample 1 (c).

C. $GaAs_{1-x}P_x$ samples

In order to extract quantitative information from the EDAFS spectra we performed either a single first shell analysis, isolating the nearest neighbor (NN) contribution by a standard Fourier filtering procedure and fitting the filtered experimental data with the experimental phases and amplitudes of bulk GaAs and GaP, and a multishell analysis on the raw data using theoretical phase shifts and amplitudes calculated *ab initio* with the GNXAS software package.[23] The theoretical atomic phase shifts and amplitudes are calculated in the muffin-tin approximation based on atom self-consistent relativistic calculations, taking into account inelastic losses through a complex Hedin-Lundqvist potential. They have been checked by fitting the spectra of bulk GaAs and GaP.

The results of the two procedures for the first shell distances of Ga-As and Ga-P are consistent within an error of 0.01 Å. It is within the accuracy of the state-of-the-art *ab initio* simulation programs on the determination of the absolute values of interatomic distances, which is known to be of approximately 0.02 Å.

The use of experimental phases and amplitudes, allows a direct comparison of the nearest-neighbor distances of the alloy with those of the bulk starting binary compounds, GaAs and GaP. The use of GNXAS program provides instead the advantage of fitting directly the raw experimental

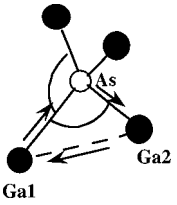

FIG. 10. Elemental tetrahedral unit indicating the MS path included in the GNXAS simulation of the data.

data, increasing the number of independent points, i.e., allowing a larger number of free parameters in the fit, and also of including MS contributions in the spectra simulation, which are important, as observed for $InAs_{1-x}P_x$ (Ref. 10) for a correct determination of the NNN distances. The MS path that can actually contribute to the signal is the three-body path Ga1-As-Ga2-Ga1, where the short paths Ga1-As and As-Ga2 correspond to the two-body NN scattering path Ga-As, and the long one Ga1-Ga2, coincides with the two-body NNN scattering path. The angle Ga1-As-Ga2 is the tetrahedral zinc-blende bond angle (see Fig. 10).

The model phases, either theoretical or experimental, were corrected according to expression (10).

As an example of the first shell analysis, the comparison of the best-fit curve with the filtered first shell signal is shown in Figs. 9(b) and 9(c) for sample 1, at the Ga and As K edges. The first shell best-fit results are reported in Table III. The average relative experimental error, calculated as reported in the previous section, is between 2.3 and 1.4 %. The fit errors have been evaluated according to the standard and criteria on EXAFS data analysis[26] doubling the normalized fit residual at minimum. The values of the Ga-As and Ga-P bond distances are the same, within the errors, for the three $GaAs_{1-x}P_x$ samples. The value obtained for the As-Ga pair, at the As *K* edge, for sample 1 is consistent within the error, with the value obtained at the Ga *K* edge. These values are very close to the bulk values (2.448 and 2.361 Å, respectively), as expected according to the well-known bimodal bond length distribution of pseudobinary semiconductor compounds. They have been measured by EXAFS on $GaAs_{1-x}P_x$ bulk alloys[27,28] as a function of P concentration, and the same values were found within the experimental errors. We should note that the error on the Ga-P distance is necessarily larger than the error on the Ga-As bond length as a result of the poor sensitivity of the fit to this parameter. This is due to the small backscattering amplitude of P for *k* values beyond 5–6 $Å^{-1}$, which makes the EDAFS frequency depending mainly on the Ga-As pair, and to the relatively low P concentration.

According to the milestone studies of Mikkelsen and Boyce on the local structure of pseudobinary semiconductor alloys,[6,27] the Ga-P and Ga-As can be evaluated as a function of their average value r_0 given by the virtual crystal approximation (VCA),

$$r_a^{\text{Ga-As}} = n_b^{\text{Ga-As}} + \Delta(r_0 - r_b^{\text{Ga-As}}),$$

$$r_a^{\text{Ga-P}} = r_b^{\text{Ga-P}} + \Delta(r_0 - r_b^{\text{Ga-P}}),$$

where r_a is the bond length in the alloy and r_b that of the binary bulk compound, and r_0 is the VCA average bond length which depends on the P concentration (x) of the alloy,

$$r_0^{\text{Ga-As}} = r_0^{\text{Ga-P}} = (1-x)r_b^{\text{Ga-As}} + x r_b^{\text{Ga-P}}.$$

The factor $\Delta = 0.25$ has been deduced for $GaAs_{1-x}P_x$ in Ref. 27 and reflects the deviation of the NN bond lengths bimodal distribution from VCA. The expected alloy values for $x = 0.22$ would be in $r_a^{\text{Ga-As}} = 2.443$ Å and $r_a^{\text{Ga-P}} = 2.377$ Å, consistent to the measured values of $r_a^{\text{Ga-As}} = 2.44 \pm 0.01$ Å and $r_a^{\text{Ga-P}} = 2.37 \pm 0.02$ Å.

In our case we do not deal exactly with a bulk alloy because the sample actually have been grown epitaxially onto a mismatched substrate with a larger lattice parameter, giving at most a tensile strain of 0.8%. Due to the large thickness of the samples, the built-in strain has partially released, breaking the epilayer and generating dislocations. However, the XRD measurements still detect a residual amount of strain acting on the lattice and one of the aims of this work was to study its effect on the interatomic distances.

The effect of the residual strain can be estimated with the help of the elastic theory[3] that relates the macroscopic elastic constants of the material with the microscopic lattice parameters. If the epilayer is still pseudomorphic, i.e., it has grown with the same in-plane lattice constant ($a_\parallel$) as the substrate, it will undergo a biaxial expansion in the growth plane and an uniaxial compression along the growth direction [001], it will loose the cubic symmetry showing a tetragonal distortion. The lattice perpendicular parameter $a_\perp$ can be calculated, according to the elastic theory, from the average VCA lattice parameter a_0 and the elastic constants of $GaAs_{1-x}P_x$, obtained from a weighted average of those of GaAs and GaP. For $x = 0.22$ we obtain

$$a_\perp = a_0 + 2(C_{12}/C_{11})(a_0 - a_\parallel) = 5.566 \text{ Å}$$

with $a_0 = (1-x)a_b^{\text{Ga-As}} + x a_b^{\text{Ga-P}} = 5.608$ Å and $a_\parallel = a_{\text{Ga-As}} = 5.654$ Å, $a_{\text{Ga-P}} = 5.451$ Å. The perpendicular and parallel strain components are defined as

$$\varepsilon_\parallel = (a_\parallel - a_0)/a_0 \text{ and } \varepsilon_\perp = (a_\perp - a_0)/a_0,$$

respectively, and are related by the C_{ij} coefficients

$$\varepsilon_\perp = -2(C_{12}/C_{11})\varepsilon_\parallel$$

for pseudomorphic $GaAs_{1-x}P_x$ with $x = 0.22$, $\varepsilon_\parallel = 0.008$, and $\varepsilon_\perp = -0.007$. Sample 2, which has an amount of in-plane strain of 0.7%, is almost pseudomorphic.

In this frame we can estimate an average strained bond length assuming that the lattice is uniformly distorted,[29]

$$r_s = 1/4(2a_\parallel^2 + a_\perp^2)^{1/2} = r_0[1 + 1/3(2\varepsilon_\parallel + \varepsilon_\perp)] = r_0 + \Delta r,$$

where $r_0 = (\sqrt{3}/4)a_0$ and Δr is the average distortion of the bond length due to the strain.

In this case it would be $\Delta r = 0.007$ Å, which added to the alloy bond lengths would give an average strained distance of

$$r_s^{\text{Ga-As}} = r_a^{\text{Ga-As}} + \Delta r = 2.450 \text{ Å},$$
$$r_s^{\text{Ga-P}} = r_a^{\text{Ga-P}} + \Delta r = 2.384 \text{ Å}.$$

Theoretical studies on $In_xGa_{1-x}As$ (Ref. 30) suggest that actually the bond-length distortion should not be the same for the two different pairs In-As and Ga-As, since the longer

TABLE IV. Multishell fit results for the $GaAs_{1-x}P_x/GaAs$ samples. ε is the residual strain and t is the film thickness. Errors have been estimated changing each parameter, while iterating the others, until the residual was doubled (Ref. 26). $\Delta r_{\text{Ga-Ga}}=0.02$ Å, and the relative errors on the σ^2 and N values are approximately 20%.

Sample	ε	t (Å)	[hkl]	$\sigma^2_{\text{Ga-P}}$ (Å^2)	$\sigma^2_{\text{Ga-As}}$ (Å^2)	$N_{\text{Ga-P}}$	$N_{\text{Ga-As}}$	$R_{\text{Ga-Ga}}$ (Å)	$\sigma^2_{\text{Ga-Ga}}$ (Å^2)	$N_{\text{Ga-Ga}}$
GaAs bulk					0.003		4	4.01	0.01	12
GaP bulk				0.008		4		3.85	0.01	12
3	0.4%	5000	[110]	0.014	0.003	0.8	2.4	3.97	0.018	9
1	0.6%	4000	[110]	0.013	0.003	1.2	2.7	3.97	0.015	12
1	0.6%	4000	$[1\bar{1}0]$	0.019	0.005	1	2.4	3.97	0.017	12
2	0.7%	600	[110]	0.008	0.003	1	3	3.99	0.017	12
2	0.7%	600	$[1\bar{1}0]$	0.008	0.004	0.3	3	4.00	0.014	12

bond is energetically more available to accommodate strain than the shorter one. On the other hand, recent measurements of the strained In-As distance on $In_xGa_{1-x}As$ (Ref. 29) point to an equal In-As/Ga-As bond distortion. If we recalculate the Δr value as in Ref. 29 applying the relative deformation to r_a instead of to r_0, $\Delta r'=r_a$, and $\frac{1}{3}(2\varepsilon_\parallel+\varepsilon_\perp)$, we obtain a different distortion for Ga-As and Ga-P

$$r_s^{\text{Ga-As}}=r_a^{\text{Ga-As}}+\Delta r'=2.455 \text{ Å},$$

$$r_s^{\text{Ga-P}}=r_a^{\text{Ga-P}}+\Delta r'=2.367 \text{ Å}.$$

In this sense the Raman measurements of Ref. 22 suggest an unequal bond-length distortion, detecting the Ga-As mode Raman shift as more sensitive to the residual strain than the Ga-P mode. Comparing with the EDAFS results we see that the Δr ($\Delta r'$) values in our samples would be at most of 0.01 Å, which is comparable to the error on distances determination, so we can only say that the bond distances of the Ga-As and Ga-P pairs remain constant as a function of residual strain; or at least they vary by less than 0.01 Å for Ga-As and 0.02 Å for Ga-P. The elastic theory shows to be for this system a good approximation to describe the strain accommodation mechanisms.

Further information on the NNN shell has been obtained by the multishell analysis. The fit parameters were as follows: the mean-square disorder in the bond length (σ^2) for the NN Ga-As/Ga-P distances, the Ga-As and Ga-P coordination numbers, the tetrahedral angle Θ and the σ^2_θ, the crossed σ^2_c (Ref. 3) and E_0. Nine parameters were at most refined, that is reasonable considering that the fit is performed on the raw EDAFS data. The coordination numbers were left free to vary as a check on the EDAFS amplitudes and also to compare the P contribution in the two different crystallographic directions. The fit results are shown in Table IV and the best-fit curves compared with the experiment in Fig. 11. The individual contributions of the different scattering paths are shown, together with the overall best-fit curve for sample 1, in Fig. 12. The third shell contribution has been included in some case in the fit but his presence cannot be considered statistically relevant due to either the signal-to-noise ratio and to the limited k range. The Θ value has been found always equal to $109.4°\pm1°$ and the σ^2_θ approximately 2°–4°. We also refined directly the Ga-Ga distance and the σ^2_r fixing Θ and σ^2_θ, obtaining the values reported in Table IV. The Ga-As and Ga-P first shell distances were fixed according to the results of the previous first shell analysis. The NNN distance values ranged from 3.96 to 4.00 Å, determined with an error of 0.02 Å. The data best fit was obtained with a single NNN distance. The second-neighbor distance Ga-Ga corresponds to two different possible paths, Ga-P-Ga and Ga-As-Ga giving a splitting of the Ga-Ga distance. It has been observed indeed in $In_xGa_{1-x}As$ and $Te_xSe_{1-x}Zn$.[6,27] In our case the two NNN distances of the starting binary compounds, 3.997 Å for GaAs and 3.854 Å for GaP, are closer to each other, if compared to $In_xGa_{1-x}As$ and $Te_xSe_{1-x}Zn$, and the relative amount of short NNN paths is quite low, being a P concentration of approximately 20%. The increased σ^2_θ and σ^2_r, with respect to the bulk binary compound values (see Table IV), can account for a significant static spread of distances around the average.

We can compare the average NNN distance obtained from the fit with the values deduced from a_0 for the relaxed alloy, and $a_\parallel$, $a_\perp$ for the pseudomorphic limit.

$$r_a^{\text{Ga-Ga}}=(\sqrt{2}/2)a_0=3.965 \text{ Å}$$

for the relaxed alloy,

$$r_{s\perp}^{\text{Ga-Ga}}=\tfrac{1}{2}(a_\parallel^2+a_\perp^2)^{1/2}=3.966 \text{ Å}$$

for the eight out-of-plane NNN atoms along the [101] and [011] directions of the cube faces,

$$r_{s\parallel}^{\text{Ga-Ga}}=r_b^{\text{Ga-Ga}}=3.998 \text{ Å}$$

for the four in-plane NNN atoms along the [110] directions. Due to the $\cos^2\theta$ factor for the [110] polarization, the two different groups of in-plane and out-of-plane are weighted the same and EDAFS will see an average value of

$$r_s^{\text{Ga-Ga}}=1/2(r_{s\perp}^{\text{Ga-Ga}}+r_{s\parallel}^{\text{Ga-Ga}})=3.982 \text{ Å}$$

that is slightly longer than the relaxed alloy value.

The values we found compare well with the predicted NNN distances. The second shell distance is even slightly larger for the almost pseudomorphic sample 2. We must ac-

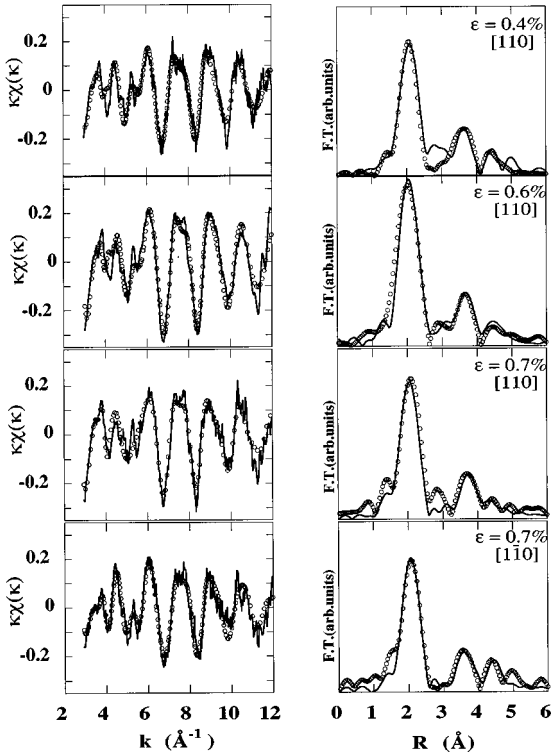

FIG. 11. Best-fit results from GNXAS program. The solid line represents the raw EDAFS data, $k^*\chi(k)$ (left column), and the correspondent FT, right column, calculated in the range 3–13 Å^{-1}. The circles represent the best-fit results. For sample 2 the best fits for the two polarization directions [110] and [1$\bar{1}$0] are shown.

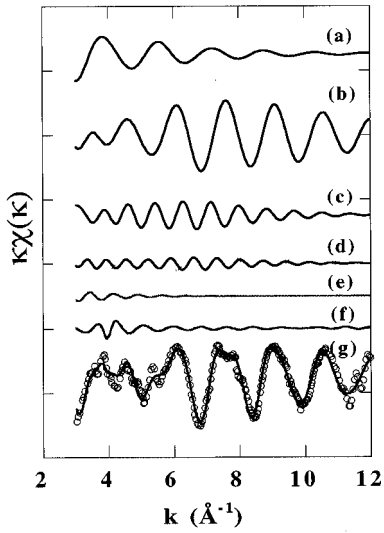

FIG. 12. Contributions of the individual scattering paths to the EDAFS spectrum. (a) Ga-As, (b) Ga-P, (c) Ga-Ga (II shell), (d) Ga-As (III shell), (e) Ga-P (III shell), (e) Ga-As-Ga (MS), (g) best fit (circles) and sample 1 raw EDAFS (solid line).

knowledge, however, that to sample such fine changes in the second shell environment, the statiscal quality of data should be improved.

The last result that we want to comment on is how the best-fit accounts for the difference between the two [110] and [1$\bar{1}$0] 006 EDAFS spectra of sample 2. First of all we should notice that the σ^2 factors of the Ga-P pair are higher for samples 3 and 1, with respect to the bulk GaP, while for sample 2 it is lower, taking a value close to the bulk compound. This sounds reasonable considering the more ordered and more ''rigid'' structure of the less relaxed sample. On the other hand, the σ^2 factors are strongly correlated with the coordination numbers and also depend on the accuracy of spectra normalization, giving a relative error bar of about 20%. Therefore the relevant numbers are the ratio $N_{\text{Ga-P}}/N_{\text{Ga-As}}$ for the two different [110] and [1$\bar{1}$0] directions, they give the concentration of P atoms around Ga. For sample 1 the two spectra are very similar to each other (see Fig. 8) and the $N_{\text{Ga-P}}/N_{\text{Ga-As}}$ ratio takes about the same value, $N_{\text{Ga-P}}/N_{\text{Ga-As}}=0.4$, giving an equal P concentration of 29%. For sample 2, the $N_{\text{Ga-P}}/N_{\text{Ga-As}}$ ratio is much lower for the [1$\bar{1}$0] orientation (0.1) than for the [110] orientation (0.33), corresponding to a P concentration of 9% and 25%, respectively, that makes the spectrum at glance more similar to pure GaAs. When switching from [110] to [1$\bar{1}$0] direction the NN atoms do not belong to the same crystallographic planes. The NN coordination number is 4 as for a powder but only two of them are sampled by the polarized beam. If the P atoms are randomly distributed or the lattice is cubic, it makes no difference, but a P ordering, joined to a deformation, could lead to a difference in the spectra.

The expected structure for these alloys is a zinc-blende disordered phase in which the cations occupy a set of fcc positions and the anions occupy randomly the other $(\frac{1}{4},\frac{1}{4},\frac{1}{4})$ shifted fcc set. Several different kinds of ordered structures have been observed in semiconductor alloys.[31]

The stability of these ordered phases is not well known, but calculations of phase diagrams of ternary alloys show narrow regions of stability for x values of approximately 0.25, 0.5, and 0.75. Calculations have also been performed using the Harrison model to calculate the strain energy[31] and to predict the strain energies and bond-lengths distribution for $In_xGa_{1-x}As$ and $GaAs_{1-x}Sb_x$. It depends on a number of factors, such as the growth mechanism, the alloy concentration, and the related amount of strain energy.

In our case we can relate the ordering effect detected by the EDAFS to the reduced thickness of sample 2, compared with sample 3 and 1, lowering the number of different ordering domains, i.e., giving an appreciable net crystallographic asymmetry. The presence of the built-in residual strain due to the mismatch with the substrates increases the ground strain energy of the randomly mixed alloy and could favor the ordered structure.

V. CONCLUSIONS

In the first part of the paper, we present the general formalism for analyzing EDAFS oscillations. The procedure is valid for any type of crystallographic structure, i.e., centrosymmetric or otherwise. The first-order EDAFS oscillations $\chi_{\mathbf{Q}}(k)$ may be expressed with a formula very similar to the EXAFS one. The EDAFS normalisation factor may be calculated using either the crystallographic structure or the parameters $\Delta\Phi=\varphi_T-\varphi_A$ and β, obtained by fitting the

DAFS spectrum with Eq. (4). For the one-anomalous-site analysis, the EDAFS crystallographic phase shift ($\varphi_0-\varphi_A$) may also be calculated with the parameters $\Delta\Phi$ and β only. Therefore, the structure is not *a priori* necessary, and a standard EXAFS analysis may be performed. However, the parameters $\Delta\Phi$ and β may not be constant as a function of energy due to the presence of a neighboring edge. In some cases, a correlation may exist between β and the scale factor and/or between $\Delta\Phi$ and the absorption correction, leading to unreliable values of β and $\Delta\Phi$. In that case, it is preferable to calculate the normalization factor and the phase shift with the crystallographic structure.

As a general trend, the DAFS spectra are very sensitive to the crystallographic DW factors. The measurements at different edges are a way to decorrelate the DW and the occupation factors of the anomalous atoms. As a matter of fact, the DAFS spectra are very sensitive to the parameter β, which is related to the products $C_{Aj}\exp(-M_{Aj}Q^2)$. Therefore, this explains the sensitivity to the DW and why measuring DAFS spectra at a few different **Q** vectors (2 or 3 for instance) can decrease appreciably the correlation between the occupation factor and the DW factor.[16]

It has been shown with the weak 006 reflection of $GaAs_{1-x}P_x$, which has a large anomalous effect, that a very small variation of the structural parameters may be detected. For the weak 006 reflection of $GaAs_{1-x}P_x$, an atomic displacement as low as one hundredth of an angstrom leads to a $\Delta\Phi$ of approximately 60°, which has been clearly evidenced by the DAFS spectra. This small variation is comparable with the variation predicted by the elastic theory, as we can deduce from the values of the lattice parameters reported in the previous section for the bulk alloy and the pseudomorphic epilayer ($a_0=5.608$ and $a_\perp=5.566$ Å, respectively). If we assume that the contraction of $a_\perp$ is linear with the strain content, the difference in $a_\perp$ between sample 3 ($\varepsilon=0.4\%$) and sample 2 ($\varepsilon=0.7\%$) should be equal to $(5.566-5.608)(0.3/0.8)$ Å $=-0.015$ Å, which would be consistent with the small contraction of 0.0096(3) Å detected by the DAFS analysis.

Using DAFS we have studied two different kinds of strained semiconductor compounds, in a different strain regime: a strained layer superlattice of $(GaP)_2(InP)_3$ and three single epilayers of $GaAs_{1-x}P_x$ ($x=0.23-0.20$) grown on a GaAs(001) substrate. In the first case, the strain is accommodated by plastic deformation of the lattice; in the second case the strain it is partially relaxed by dislocation generation leaving a certain amount of residual strain in the lattice.

We can draw three main results about the local microscopic structure of the two systems. First, we measure an elongation of 0.04 Å of the Ga-P bond length in the SLS sample. Since this elongation agrees with elastic theory, the theory still holds for very thin epilayers (2 ML) with a high strain content (3.6%). In this sense, the results reported in literature are not yet very clear; deviations have been observed for buried single layers of InAs (Ref. 32) and for $InGa_{1-x}As_x$ epilayers with a thickness lower than 10 Å,[33] whereas elastic deformation has been observed on a 2-ML InAs/GaAs sample.[33] Our results have added information on a real SLS system in which the short-range order could not be studied by any other EXAFS-like approach.

Second, concerning the $GaAs_{1-x}P_x$ samples, the Ga-As and Ga-P bond distances ($r_{\text{Ga-As}}=2.44\pm0.01$ Å and $r_{\text{Ga-P}}=2.37\pm0.02$ Å) do not vary, within the standard deviation, as a function of residual strain, remaining very close to the correspondent bulk value of the starting binary compounds as was observed for the relaxed pseudobinary alloy.[6,27] The next-nearest-neighbor distances obtained by a multishell analysis of the raw EDAFS data compare well with the values predicted for the relaxed and pseudomorphic alloy.

Third, we compare EDAFS spectra of two $GaAs_{1-x}P_x$ samples recorded with two different orientations of the x-ray polarization vector. The most strained and thinnest sample shows a difference in the low-k region of the spectrum (which is more sensitive to the presence of P atoms) when switching the x-ray polarization from [110] to $[1\bar{1}0]$ direction. The multishell fit analysis indicates that for the $[1\bar{1}0]$ direction, the number of P atoms seen by the Ga absorber is much lower, as deduced qualitatively by comparing the two spectra with the GaP and GaAs bulk measurements. That result can be understood in terms of a partial P ordering mechanism along the [001] growth direction, which has been observed in analogous pseudobinary alloys and explained theoretically in terms of strain energy.[31]

ACKNOWLEDGMENTS

We are grateful to the staff of the French CRG-D2AM beamline for providing us assistance during the experiments, and to the CSIC-Instituto de Microelectronica de Madrid for providing the samples and performing the XRD characterization. A special thanks to Vassileios Dalakas, who helped us to set up the analysis program at the CNRS laboratory of Crystallography. This work was supported by the Laboratoires Européens Associés (LEA) for solid state materials research by means of neutron and synchrotron beam based techniques (MA.NE.S), by DGICYT Project No. PB-94-0022-C02-01, and by CICYT Project No. MAT96-0491.

*Author to whom correspondence should be addressed. Electronic address: renevier@polycnrs-gre.fr

[1] See, for example, T. R. Chen, Y. H. Zhuang, L. E. Eng, and A. Yariv, Appl. Phys. Lett. **57**, 2402 (1990); Jae-Hoon Kim, A. Larsson, and L. P. Lee, Appl. Phys. Lett. **58**, 7 (1991).

[2] See, for example, *Strained Layer Superlattices Physics*, edited by T. Pearsall (Academic, New York, 1990).

[3] J. Hornstra and W. J. Bartels, J. Cryst. Growth **14**, 518 (1979).

[4] B. W. Dodson, J. V. Tsao, S. T. Picraux, and D. M. Cornelison, Phys. Rev. Lett. **59**, 2455 (1987); P. M. J. Marée, J. C. Barbour, and J. F. Van der Veen, J. Appl. Phys. **62**, 4413 (1987).

[5] Y. Cai and M. F. Thorpe, Phys. Rev. B **46**, 15 872 (1992).

[6] J. C. Mikkelsen Jr. and J. B. Boyce, Phys. Rev. B **28**, 7130 (1983).

[7] A. Balzarotti, M. Czyzyk, A. Kisiel, N. Motta, M. Podgorny, and M. Zimnal-Starnawsha, Phys. Rev. B **30**, 2295 (1984).

[8] H. Oyanagi, Y. Takeda, T. Matsushita, T. Ishiguro, T. Yao, and A. Sasaki, Solid State Commun. **67**, 453 (1988).

[9] C. Lamberti, S. Bordiga, F. Boscherini, S. Pascarelli, and G. M. Schiavini, Appl. Phys. Lett. **64**, 1430 (1994); C. Lamberti, S.

Bordiga, F. Boscherini, S. Pascarelli, G. M. Schiavini, C. Ferrari, L. Lazzarini, and G. Salviati, J. Appl. Phys. **76**, 4581 (1994).
[10] S. Pascarelli, F. Boscherini, C. Lamberti, and S. Mobilio, Phys. Rev. B **56**, 1936 (1997).
[11] M. G. Proietti, S. Turchini, J. Garcia, G. Lamble, F. Martelli, and T. Prosperi, J. Appl. Phys. **78**, 6574 (1995).
[12] M. G. Proietti, S. Turchini, F. Martelli, J. Garcia, T. Prosperi, D. Chandesris, and J. Vogel, J. Phys. IV **7**, C2-697 (1997).
[13] J. C. Woicik, J. G. Pellegrino, S. H. Southworth, P. S. Shaw, B. A. Karlin, C. E. Bouldin, and K. E. Miyano, Phys. Rev. B **52**, R2281 (1995).
[14] H. Stragier, J. O. Cross, J. J. Rehr, L. B. Sorensen, C. E. Bouldin, and J. C. Woicik, Phys. Rev. Lett. **21**, 3064 (1992); S. Sorensen, in *Resonant Anomalous X-ray Scattering*, edited by G. Materlik, C. J. Sparks, and K. Fisher (North-Holland, Amsterdam, 1994).
[15] I. J. Pickering, M. Sansone, J. Marsch, and G. N. George, J. Am. Chem. Soc. **115**, 6302 (1993).
[16] H. Renevier, J. L. Hodeau, P. Wolfers, S. Andrieu, J. Weigelt, and R. Frahm, Phys. Rev. Lett. **78**, 2775 (1997).
[17] H. Renevier, J. Weigelt, S. Andrieu, R. Frahm, and D. Raoux, Physica B **208-209**, 217 (1995).
[18] I. Arcon, A. Kodre, D. Glavic, and M. Hribar, J. Phys. (Paris), Colloq. **48**, C9-1105 (1987).
[19] J. O. Cross, Ph.D. thesis, University of Washington, 1996.
[20] J. Vacinova, J. L. Hodeau, P. Wolfers, J. P. Lauriat, and E. Elkaïm, J. Synchrotron Radiat. **2**, 236 (1995); J. L. Hodeau, J. Vacinova, P. Wolfers, Y. Garreau, A. Fontaine, M. Hagelstein, E. Elkaïm, A. Collomb, and J. Muller, Nucl. Instrum. Methods Phys. Res. B **97**, 115 (1995).
[21] D. C. Meyer, K. Richter, P. Paufler, and H. G. Krane, Cryst. Res. Technol. **29**, K66 (1994).
[22] G. Armelles, M. L. Sanjuá, L. Gonzalez, and Y. Gonzalez, Appl. Phys. Lett. **68**, 1805 (1996).
[23] A. Filipponi, A. Di Cicco, and C. R. Natoli, Phys. Rev. B **52**, 15 122 (1995); and A. Di Cicco, *ibid.* 15 135 (1995).
[24] F. Briones, L. Gonzalez, and A. Ruiz, Appl. Phys. A: Solids Surf. **49**, 729 (1989); Y. Gonzalez, L. Gonzalez, and F. Briones, J. Vac. Sci. Technol. A **13**, 73 (1995).
[25] J. L. Ferrer, J. P. Simon, J. F. Berar, B. Caillot, E. Fanchon, O. Kaikati, S. Arnaud, M. Guidotti, M. Pirocchi, and M. Roth, J. Synchrotron Radiat. **5**, 1346 (1998).
[26] Reports of the *International Workshop on Standards and Criteria in Absorption X-Ray Spectroscopy, Brookhaven National Laboratory, 1988*, edited by F. W. Lytle, D. E. Sayers, and E. A. Stern [Physica B **158**, 701 (1989)].
[27] J. B. Boyce and J. C. Mikkelsen, J. Cryst. Growth **98**, 37 (1989).
[28] T. Sasaki, T. Onda, R. Ito, and N. Ogasawara, Jpn. J. Appl. Phys., Part 1 **25**, 231 (1986).
[29] J. C. Woicik, J. G. Pellegrino, B. Steiner, K. E. Miyano, S. G. Bompadre, L. B. Sorensen, T.-L. Lee, and S. Khalid, Phys. Rev. Lett. **79**, 5026 (1997).
[30] A. Amore Bonapasta and G. Scavia, Phys. Rev. B **50**, 2671 (1994).
[31] See K. E. Newman, J. Shen, and D. Teng, Superlattices Microstruct. **6**, 245 (1989), and references therein.
[32] O. Brandt, K. Ploog, R. Bierwolf, and M. Hoehenstein, Phys. Rev. Lett. **68**, 1339 (1992).
[33] E. Bergignat, M. Gendry, G. Hollinger, and G. Grenet, Phys. Rev. B **49**, 13 544 (1994). (1996).